THE JOURNAL OF PHYSICAL CHEMISTRY B

Article

pubs.acs.org/JPCB

Optimizing Electrostatic Field Calculations with the Adaptive Poisson−Boltzmann Solver to Predict Electric Fields at Protein−Protein Interfaces II: Explicit Near-Probe and Hydrogen-Bonding Water Molecules

Andrew W. Ritchie and Lauren J. Webb*

Department of Chemistry, Center for Nano- and Molecular Science and Technology, and Institute for Cell and Molecular Biology, The University of Texas at Austin, 1 University Station, A5300, Austin, Texas 78712, United States

Supporting Information

ABSTRACT: We have examined the effects of including explicit, near-probe solvent molecules in a continuum electrostatics strategy using the linear Poisson−Boltzmann equation with the Adaptive Poisson−Boltzmann Solver (APBS) to calculate electric fields at the midpoint of a nitrile bond both at the surface of a monomeric protein and when docked at a protein−protein interface. Results were compared to experimental vibrational absorption energy measurements of the nitrile oscillator. We examined three methods for selecting explicit water molecules: (1) all water molecules within 5 Å of the nitrile nitrogen; (2) the water molecule closest to the nitrile nitrogen; and (3) any single water molecule hydrogen-bonding to the nitrile. The correlation between absolute field strengths with experimental absorption energies were calculated and it was observed that method 1 was only an improvement for the monomer calculations, while methods 2 and 3 were not significantly different from the purely implicit solvent calculations for all protein systems examined. Upon taking the difference in calculated electrostatic fields and comparing to the difference in absorption frequencies, we typically observed an increase in experimental correlation for all methods, with method 1 showing the largest gain, likely due to the improved absolute monomer correlations using that method. These results suggest that, unlike with quantum mechanical methods, when calculating absolute fields using entirely classical models, implicit solvent is typically sufficient and additional work to identify hydrogen-bonding or nearest waters does not significantly impact the results. Although we observed that a sphere of solvent near the field of interest improved results for relative field calculations, it should not be consider a panacea for all situations.

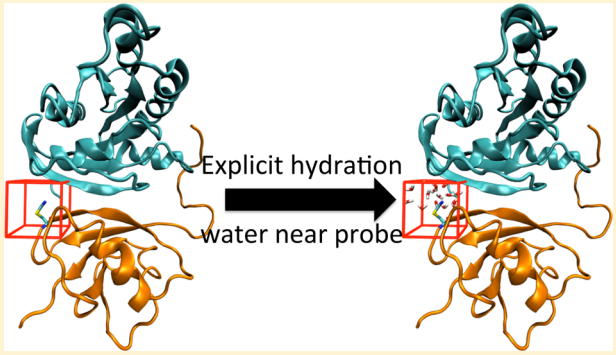

INTRODUCTION

Quantitative calculations of electrostatic fields in biological molecules are ubiquitous throughout the biophysical literature in aiding many types of investigations, but their accuracy has proven difficult to confirm from experimental measurements.[1−31] We have previously reported the accuracy of calculated protein electrostatic fields determined by docking various functional mutants of the protein Rap1a to six different constructs of the downstream effector protein Ral guanosine dissociation inhibitor carrying a cyanocysteine vibrational probe (hereafter referred to as Rap and RalGDS, respectively) using the linear Poisson−Boltzmann equation (LPBE).[32] In these calculations, the electrostatic potential, $\phi(\vec{r})$ (given as a function of the position vector $\vec{r}$), is dependent on the spatially resolved dielectric constant, $\varepsilon(\vec{r})$, the ion accessibility coefficient, $\bar{\kappa}$, and the charge distribution density, $\rho(\vec{r})$:[33]

$$\nabla \bullet \varepsilon(\vec{r})\nabla\phi(\vec{r}) = \varepsilon(\vec{r})\vec{\kappa}^2\phi(\vec{r}) - 4\pi\rho(\vec{r}) \quad (1)$$

For complex geometric shapes, such as a protein, the LPBE cannot be solved analytically. Instead, the LPBE is solved numerically by discretizing atomic partial charges and the local dielectric to a grid and solving using finite element or multigrid methods to perform a series of single-point LPBE calculations to obtain the numeric potential at each grid point.[34−36] A numerical electrostatic field is then obtained by taking the negative gradient of the calculated potential. This numerical solution to the LPBE is hereafter referred to as the numeric method.

We previously presented how changes in (1) the calculation method, (2) the box size and grid point density, and (3) the box location affected the observed correlation to experimental

Special Issue: James L. Skinner Festschrift

Received: September 16, 2013
Revised: December 23, 2013

   dx.doi.org/10.1021/jp4092656 | J. Phys. Chem. B XXXX, XXX, XXX−XXX

data. For example, the solvent reaction field (SRF), shown in eq 2, can be computed from the difference between the gradients of the electrostatic potential calculated with different values for the protein and solvent dielectrics, $\varepsilon_{protein}$ and $\varepsilon_{solvent}$, respectively:

$$\mathrm{SRF} = \frac{-\partial}{\partial \vec{r}}\phi(\vec{r})_{(\varepsilon_{protein}\neq\varepsilon_{solvent})} - \frac{-\partial}{\partial \vec{r}}\phi(\vec{r})_{(\varepsilon_{protein}=\varepsilon_{solvent})} \tag{2}$$

The SRF can be solved numerically using the LPBE to average out solvent effects to the total electrostatic field and take advantage of the less-rigorous solvent sampling requirement of an implicit solvent model. The numerical SRF is then added to the analytic Coulombic protein field, shown in eq 3, where ε_0 is the permittivity of free space, $\varepsilon_{protein}$ is the protein dielectric, q_i is the charge on atom i, $\vec{r}$ is the vector from atom i to the location of interest, and $\hat{r}$ is the unit vector of $\vec{r}$.

$$F_{coulomb}(\vec{r}) = \frac{1}{4\pi\varepsilon_0}\frac{1}{\varepsilon_{protein}}\sum_i \frac{q_i\hat{r}}{\vec{r}^{\,3}} \tag{3}$$

In the previous study, we looked at different calculation methods by comparing the sum of the numeric solvent field and the analytic protein field, which we called the reaction field method, to the numeric method. We determined that the reaction field method yielded the highest correlation to experimentally observed vibrational frequencies for absolute field calculations with a box centered on the nitrile, regardless of box size and grid point density.[37] Changes in the experimentally observed vibrational absorption frequencies were best correlated to changes in the numeric total field calculations with a box centered on the nitrile, also regardless of box size and grid point density. Both trends were linearly correlated to vibrational absorption frequencies, as expected due to the vibrational Stark effect (VSE), shown in eq 4, where $\Delta\vec{\mu}$ is the difference dipole or Stark tuning rate, $\Delta\vec{\nu}$ is the change in vibrational absorption energy, and $\Delta\vec{F}$ is the change in external electric field experienced by the vibrational chromophore.[38−44]

$$\Delta E = hc\Delta\vec{\nu} = -\Delta\vec{\mu}\bullet\Delta\vec{F} \tag{4}$$

For our thiocyanate vibrational probe, the Stark tuning rate is 0.77 $cm^{-1}/(MV\ cm^{-1})$ = 1.99 $cm^{-1}/(k_bT/eÅ)$.

The LPBE is an implicit solvent, continuum electrostatic model subject to approximations about the dielectric environment that have already been discussed at length.[5,24−26,32,45] A second approximation, however, is the difference between bulk water, modeled implicitly as a dielectric of 78, and water that is structurally or chemically important in the system. In our previous work, all solvent was treated as bulk solvent and all explicit references to solvent atoms were removed from structures prior to solving the LPBE. However, it is known that bulk water is distinct from water that is interacting with the surface of the protein, and is identified as so-called hydration water.[46−49] Hydration water is less mobile than bulk water, has a lower dielectric constant than bulk water,[50] and can play a role in stabilizing protein−protein or protein−ligand interactions.[51,52] Dismissing these persistent waters as part of the bulk solution may be detrimental to the quality of calculations of various properties that depend on molecular structure and charge such as electrostatic potentials and fields. To address this, Layfield et al.[19] recently demonstrated the importance of explicit inclusion of the water molecule nearest the nitrile probe in a quantum mechanical calculation of the vibrational frequency of nitrile probes. The included water molecule helped account for polarization effects of the solvent and improved the accuracy of their calculated vibrational shifts. Additionally, Fennell et al.[53] showed that employing an implicit solvent model that distinguishes between bulk water and hydration water can better account for solvation shell properties than a purely implicit solvent model and yields results consistent with explicit treatments.

Our previous work compared calculated electrostatic fields to experimentally measured vibrational absorption frequencies for six nitrile probes placed along the Rap/RalGDS interface, at positions $N27C_{SCN}$, $G28C_{SCN}$, $N29C_{SCN}$, $Y31C_{SCN}$, $K32C_{SCN}$, and $N54C_{SCN}$, for monomeric RalGDS[42] as well as these mutants of RalGDS docked to WT Rap, Rap E30D, Rap K31E, and Rap E30D/K31E.[41] This constitutes a set of experiments in which the exact quantity we are trying to calculate, the electrostatic field at the vibrational chromophore, is being directly measured via the VSE. In the work reported here, we test whether including explicit water molecules improves computational correlation to experiment compared to the original, purely implicit solvent calculations in a purely classical continuum electrostatics calculation.

METHODS

Molecular Dynamics Simulations. The sampling strategy has previously been described in detail.[32] Briefly, using the Amber03 force field[54] in Gromacs,[55−58] a two-dimensional umbrella sampling strategy was used to fully sample the χ_1 and χ_2 rotamers of the unnatural amino acid, cyanocysteine, at each of six different probe locations on RalGDS ($N27C_{SCN}$, $G28C_{SCN}$, $N29C_{SCN}$, $Y31C_{SCN}$, $K32C_{SCN}$, and $N54C_{SCN}$) in the monomeric form and docked to one of the various constructs of Rap: WT, E30D, K31E, and the E30D/K31E double mutant. These systems were chosen to be contiguous with our previous study. A total of 144 starting structures, one for each permutation of χ_1 from 0 to 330° in 30° steps and χ_2 from 0 to 330° in 30° steps, were sampled for 400 ps with a quadratic biasing potential of 70 kJ mol^{-1} rad^{-2} in each dimension following the typical MD solvation, charge balancing, and relaxation protocols. Frames were saved every 5 ps, resulting in 57.6 ns of simulation and 11664 frames for each system. The biased simulations were then deconvoluted using the weighted histogram analysis method (WHAM)[59,60] to construct a torsional potential of mean force (PMF) profile, which is related to the torsional probability density distribution by the Boltzmann distribution and partition function, shown in eq 5.

$$P_i = \frac{e^{-\beta\cdot \mathrm{PMF}_i}}{\sum_{j=0}^{N} e^{-\beta\cdot \mathrm{PMF}_i}},\quad \beta = \frac{1}{k_bT}$$

$$\langle E\rangle = \sum_{i=0}^{N} P_iE_i \tag{5}$$

In total, 1728 μs of simulation were performed on 30 total protein systems.

Continuum Solvent Electrostatics Calculations. The electrostatic calculation strategy has previously been described in detail.[32] In summary, we have previously observed that for the absolute field calculations, the highest correlation to

dx.doi.org/10.1021/jp4092656 | J. Phys. Chem. B XXXX, XXX, XXX−XXX

experiment was obtained when the reaction field method was used to calculate electrostatic fields.[32] In the difference field calculations, the highest correlation was observed when using the numeric method. In both cases, higher grid densities and boxes centered on the nitrile most consistently yielded the highest correlations. The calculation strategy used here is identical to those optimized parameters.

The electrostatic field was calculated for each frame by solving the LPBE at 300 K using a two-stage, multigrid, manual focusing strategy (APBS keyword "mg-manual") twice, as per eq 2: once with a solvent dielectric of 78 and a solute dielectric of 2 and once with the solvent dielectric and solute dielectric both set to 2, followed by calculating the projection of the Coulomb field at the nitrile midpoint along the nitrile bond vector, then summing eqs 2 and 3. A Boltzmann-weighted average was calculated by summing the product of the frame's probability and the frame's electrostatic field. For the first stage calculation, the system was centered in a 240 × 240 × 240 $Å^3$ box with 97 grid points in each dimension. To solve the second order differential equation, a single Debye−Hückel boundary condition was used. To account for buffer in solution, 0.150 M^{+1} charge ions and 0.150 M^{-1} charge ions, both with 2.0 Å radii, were included. The first-stage box provided the boundary conditions for the second-stage box. The second-stage box was centered on the nitrile Cδ with dimensions of 10^3 $Å^3$ and 193 grid points in each dimension (GS = 0.052 Å/grid point). Water oxygen molecules were treated as part of the low-dielectric region, with an atomic radius of 1.6612 Å, while water hydrogen atoms were given a radius of zero, both consistent with the Amber99 TIP3P water from the AMBER.DAT parameter file for pdb2pqr.[61,62]

Frame Selection, Water Selection, and Preparation. All structures examined had a total of 56.7 ns of simulation with frames saved every 5 ps, resulting in 11664 frames in which we solved the LPBE. Since the goal of our investigation is to find an easy, generalizable way to calculate electrostatic fields representative of the VSE, one of our criteria is to limit the number of arbitrary user-choices in the calculation, such as frame picking. Therefore, we used all of the frames saved when calculating our Boltzmann-weighted distributions and averages.

We examined three different methods for selecting individual water molecules to be included in the explicit portion of the calculation: (1) all water within 5 Å of the nitrile Nε atom; (2) the water molecule closest to the nitrile Nε atom; and (3) any water molecules hydrogen-bonding to the nitrile Nε atom. Frames were prepared using the GROMACS g_select utility in conjunction with trjconv to remove all solvent that was more than 15 Å away from the nitrile Nε. Each frame was further processed using Python scripts to generate a .pqr file containing explicit water molecules selected through each of the three methods. For example, Figure 1 shows a 5 Å solvent sphere for a representative snapshot of RalG28C_{SCN} docked to WT Rap. We chose a 5 Å radius sphere because it is large enough that it will include any waters significantly interacting with the nitrile. The sphere was centered on the Nε rather than the Cδ of the nitrile because the nitrogen can act as a hydrogen-bond acceptor and we want to be sure to capture those water molecules should this be occurring in the simulation. We considered a water molecule to be hydrogen-bonded to the nitrile if the Nε···H separation was ≤2.25 Å and the Nε−H−O smallest angle was ≥138°. These definitions were chosen to reach the extremes of the nitrile-water parameters reported by Le Questel et al.[63] For both the 5 Å sphere and hydrogen-bonding methods, if a frame did not have a water molecule fitting the respective criteria, no explicit water molecules were included and the LPBE solutions from the original, entirely implicit calculations were used for that frame. Each 5 Å sphere frame could contain zero (∼1.4% of frames), one (∼2.7% of frames), or more (∼95.9% of frames) water molecules in the frame. Each nearest water frame was guaranteed to have exactly one water molecule. Each hydrogen-bonding water frame could have exactly zero (∼89.3% of frames) or exactly one (∼10.7% of frames) water molecule in each frame.

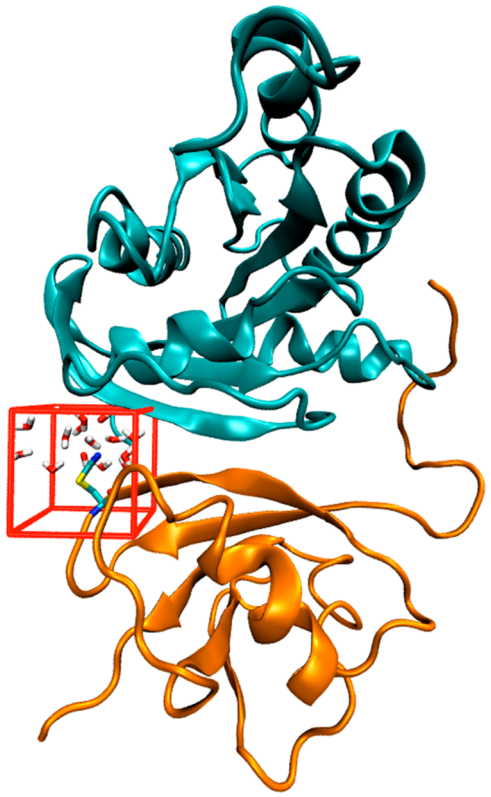

Figure 1. Representative snapshot of RalGDS G28C_{SCN} docked to WT Rap demonstrating the size of the 10^3 $Å^3$ second-stage box (red) used to calculate the electrostatic field in APBS and showing water molecules within 5 Å of the nitrile Nε.

RESULTS AND DISCUSSION

A. Calculations of Absolute Fields. Figures 2 and 3 and Supporting Information Figures S1−S3, compare the calculated electrostatic fields at the nitrile bond midpoint projected along the nitrile bond vector using the various partially explicit solvent methods (blue) to the experimentally observed nitrile vibrational absorption frequencies for the RalGDS monomer, RalGDS docked to WT Rap, and RalGDS docked to Rap E30D, K31E, and E30D/K31E, respectively, and compared to previous results obtained with no explicit water molecules (red). Results using both the numeric LBPE solutions (left column) as well as the reaction field method (right column) are presented. Error bars have been omitted for clarity, but we consistently observed standard deviations of the electrostatic field calculations of approximately ±6.5 k_bT/eÅ and for vibrational frequencies ranging from about ±1 cm^{-1}. The reaction field method yielded higher correlation to experiment than the numeric solutions, consistent with our previously reported results. Because of this, further discussion of the

dx.doi.org/10.1021/jp4092656 | J. Phys. Chem. B XXXX, XXX, XXX−XXX

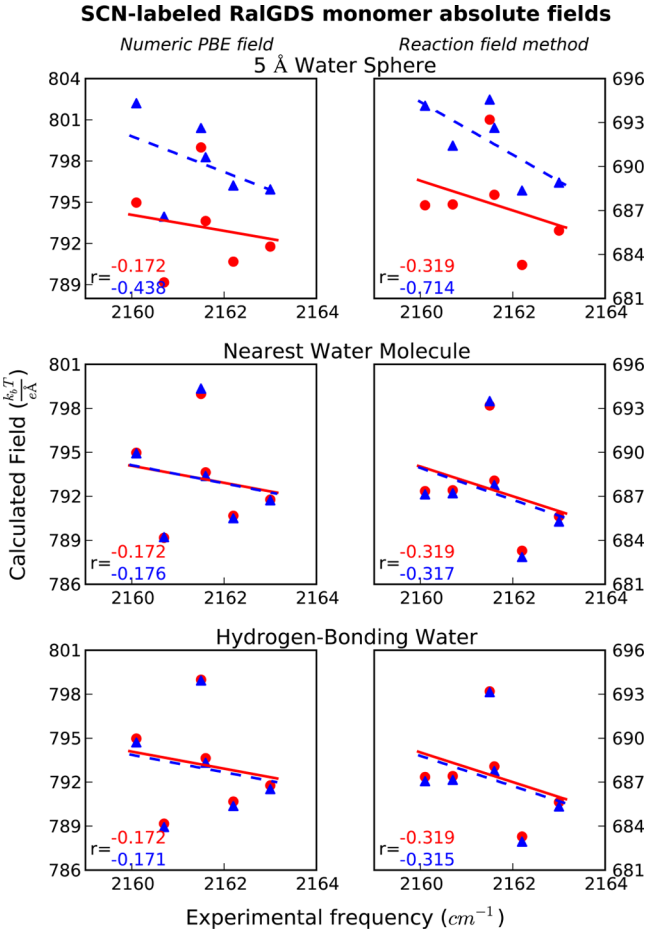

Figure 2. Absolute field calculations using the numeric LPBE solutions (left column) and the numeric reaction field method (right column) compared to the experimental frequencies for various nitrile probe locations on the RalGDS monomer. Red: originally reported, entirely implicit solvent fields; blue: fields using the solvent selection model described by the row subheading. Correlation coefficients are listed in the bottom left corner in the corresponding color. Standard deviations are approximately ±1 cm^{-1} and ±6.5 k_bT/eÅ.

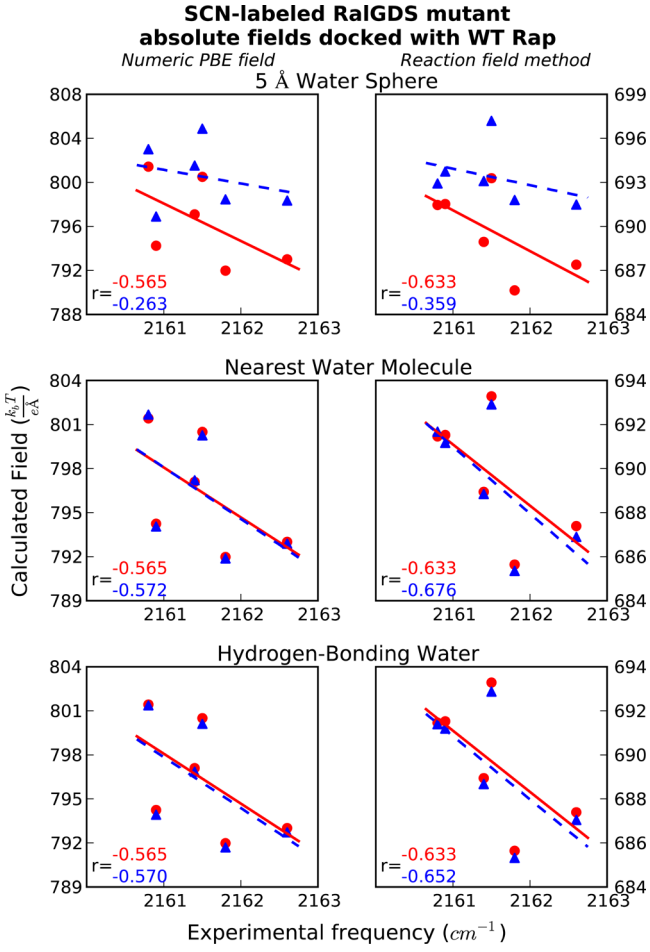

Figure 3. Absolute field calculations using the numeric LPBE solutions (left column) and the numeric reaction field method (right column) compared to the experimental frequencies for various nitrile probe locations on RalGDS docked to WT Rap. Red: originally reported, entirely implicit solvent fields; blue: fields using the solvent selection model described by the row subheading. Correlation coefficients are listed in the bottom left corner in the corresponding color. Standard deviations are approximately ±1 cm^{-1} and ±6.5 k_bT/eÅ.

results of the absolute calculations will be limited to the reaction field method.

5 Å Sphere. The top rows of Figures 2 and 3 and Supporting Information Figures S1–S3, show the electrostatic fields calculated when all water molecules within 5 Å of the nitrile Nε atom are explicitly included. In all cases the reaction field method yields better correlation than the numeric method. In Figure 2, the monomeric RalGDS field correlations are significantly improved by the inclusion of the solvent sphere and yet in every docked system, the solvent sphere detracts from the overall correlation to experiment.

To understand this observation, we looked at each water molecule within 5 Å of the nitrile Nε and determined the probability of a water molecule staying within 5 Å of the nitrile for *n* frames (*n* ranging from 1 to 81, the number of frames in each trajectory), shown for the RalGDS monomer in Figure 4, as well for RalGDS docked to the various Rap constructs (Supporting Information Figures S4–S7). In each figure, the probe location is listed as the subtitle to each histogram and the trajectory average number of frames (not a Boltzmann-weighted average) listed in the upper-right corner. The error bar on each bin is the standard deviation among the 144 trajectories for that bin. These averages are also tabulated in Table 1. We observed that the RalGDS monomers have the lowest average number of frames that each water molecule is within the solvent sphere (15.6), while the docked complexes average approximately 18–20 frames, indicating that there is more water moving in-and-out of the simulated system for the monomers than for the dimers.

The improvement in experimental correlation seen (Figure 2) using the 5 Å explicit solvent spheres (blue) compared to the entirely implicit solvent model (red) for *only* the RalGDS monomers and not the docked complex (Figure 3) may be an artifact of insufficient water sampling in the docked simulations. Not only do the RalGDS monomers have fewer atoms, and thus fewer degrees of freedom to sample, but the docked complexes also have the Rap constructs in close proximity to the nitrile probes. One of the advantages of an implicit solvent model is the effects of the solvent are treated as an average, bulk property, and are not limited by poor sampling. When using explicit solvent, care must be taken to ensure the solvent is fully relaxed and sampled. The significant translational and rotational mobility of each water molecule requires a significant amount of simulation time to fully sample. By explicitly including some

dx.doi.org/10.1021/jp4092656 | J. Phys. Chem. B XXXX, XXX, XXX–XXX

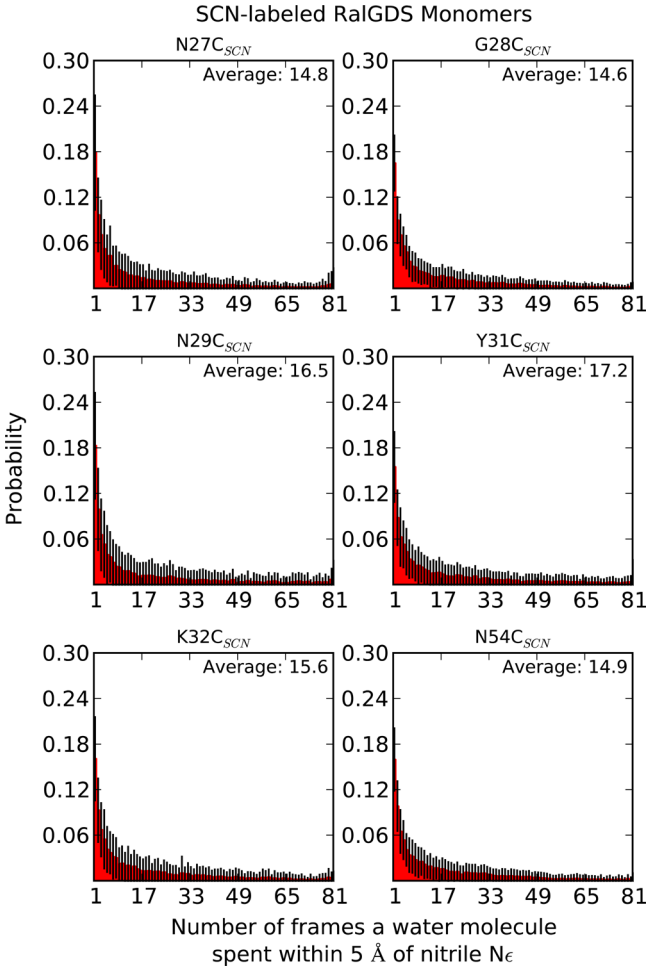

Figure 4. Observed probability of a water molecule being within 5 Å of the nitrile Nε for some number of frames in the simulation for various probe locations on the RalGDS monomer. The error bar on each bin is the standard deviation among the 144 trajectories for that bin.

water molecules, we were able to observe more water molecules trapped in local minima created by interactions with Rap than in the monomer calculations. This can be seen in Figure 4 and Supporting Information Figures S4–S7, as the spike in the probability of water molecules staying within the solvent sphere for all 81 snapshots of each 400 ps simulation, such as in the K32C$_{SCN}$ RalGDS mutant docked to WT Rap (Supporting Information Figure S4, lower-left corner).

The primary criteria for convergence of our simulations were (1) good sampling of the thiocyanate χ_1 and χ_2 dihedral rotamers and (2) the numeric reaction field with entirely implicit solvent ceasing to change significantly with additional sampling time.[32] Neither of these criteria are significantly dependent on the water being well sampled. A similar study by Fried et al.[64] compared vibrational frequencies of a carbonyl oscillator to the solvent electrostatics by performing 2 ns of simulation on a solvated small molecule and 20 ns of simulation on a solvated protein (ribonuclease S) in order to obtain well-sampled solvent. In contrast, we performed 144 × 400 ps simulations using an enhanced molecular dynamics strategy targeted at the probe only. For the solvent, backbone, and all noncyanocysteine side chains, a relatively small amount of time was allowed for exploring the free energy landscape; this is a known limitation of the enhanced sampling method used, which we accepted based on the hypothesis that the most significant degree of freedom in our system is the nitrile orientation.

To test our system for convergence, we calculated the Boltzmann-weighted average field at each time step $n\Delta t$, where Δt is 0.72 ns and n ranged from 1 to 80 (the number of frames in each trajectory) for all 30 systems examined. Briefly, we used WHAM at each time step to calculate new weights after each additional time step of each trajectory (0.005 ns per step trajectory, 144 trajectories for a total of 0.72 ns per step). Using the new weights and the frames present in calculating them, a Boltzmann-weighted average field was calculated for the 5 Å solvent sphere using both the numeric field method as well as the reaction field method. The average field as a function of time, relative to the average field at time $n\Delta t = 0$, is shown in Supporting Information Figure S8. The field relative to the initial field was chosen to allow easy visualization using a single y-axis of the average field calculated using the numeric field method (blue) and the reaction field method (green). Relative to the magnitude of the standard deviation in field, the average field did not change significantly after the first half of the simulation in nearly all systems. To further show this feature, we have plotted the derivative with respect to time of the average field at each time step in Figure 5. This was obtained from the finite difference between steps. In the first one-third to one-half of the simulation, the field gradient changed rapidly as t increased, but by the last half of the simulation, the field gradient showed only small fluctuations centered about zero, indicating that, on average, each additional time step is not changing the calculated average significantly. Given this information, it is reasonable to conclude that, even with explicit water near the probe, each additional time step is not significantly altering the average calculated field and the simulation has converged with respect to the electrostatic field experienced by the nitrile probe, the relevant experimental parameter.

Table 1. Average[a] Number of Frames Water Molecules Remained within 5 Å of the Nitrile Nε Atom, Along with the Average and Standard Deviations, for the Monomeric RalGDS and RalGDS Bound to Various Rap Constructs

	monomer	WT	E30D	K31E	E30D/K31E
N27C$_{SCN}$	14.8	16.2	13.2	16.8	15.1
G28C$_{SCN}$	14.6	17.0	16.9	16.9	18.2
N29C$_{SCN}$	16.5	21.5	20.6	23.5	23.4
Y31C$_{SCN}$	17.2	19.5	19.1	17.2	18.3
K32C$_{SCN}$	15.6	27.8	22.0	24.7	22.7
N54C$_{SCN}$	14.9	18.6	18.8	16.9	18.4
avg[a]	15.6 ± 1.0	20.1 ± 4.2	18.4 ± 3.1	19.3 ± 3.7	19.3 ± 3.1

[a]Not a Boltzmann-weighted average.

dx.doi.org/10.1021/jp4092656 | J. Phys. Chem. B XXXX, XXX, XXX−XXX

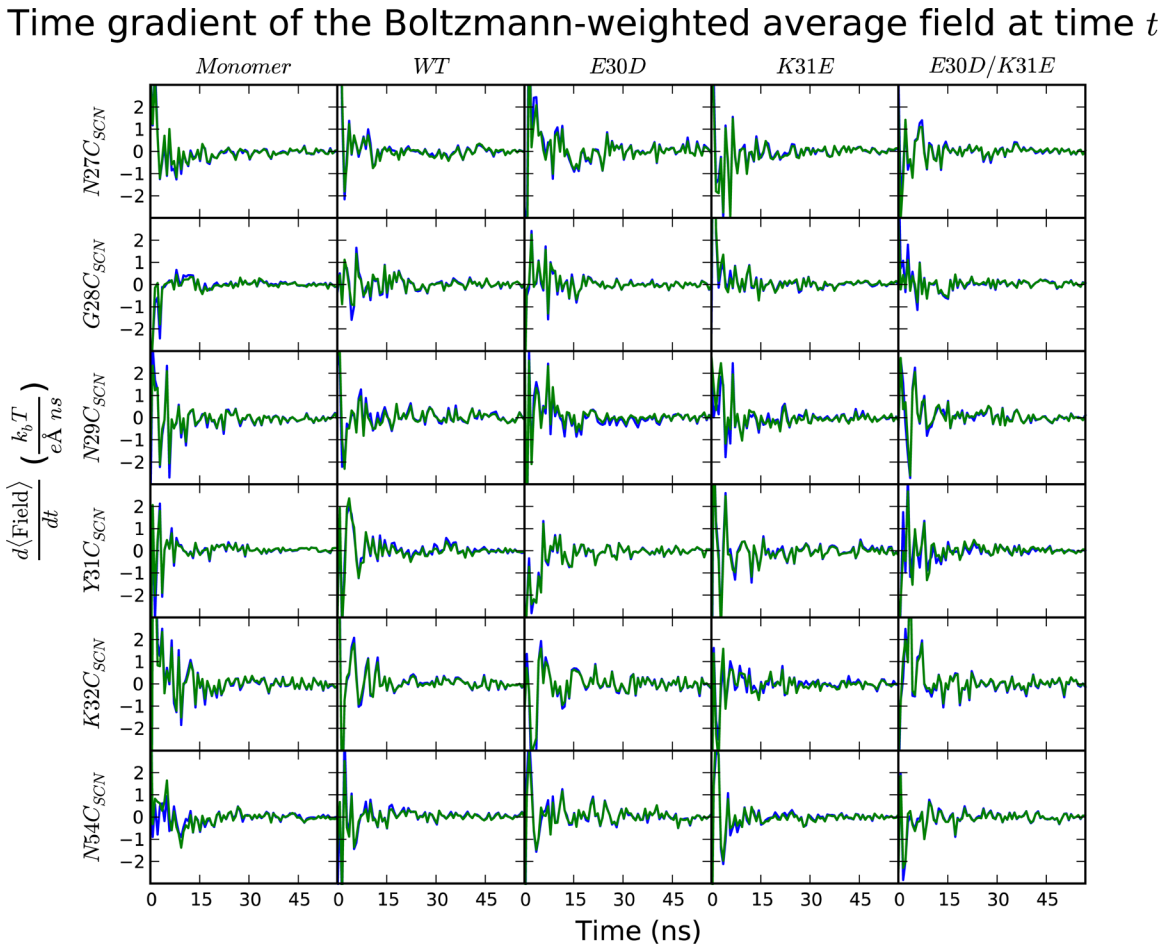

Figure 5. First derivative with respect to time of the Boltzmann-weighted average field at each time step for the various Rap and RalGDS constructs: green, numeric field method; blue, reaction field method.

Using APBS and treating all water molecules implicitly yielded better correlations to experimental data than treating water molecules within 5 Å of the nitrile probe explicitly in all the docked simulations given identical sampling strategies. The typical, entirely implicit, solvent treatment outperforms this selectively explicit solvent treatment at similar computational costs. Allowing adequate simulation time for the explicit solvent to be fully sampled, the 5 Å solvent sphere calculations and the entirely implicit solvent calculations should give identical results. If the entirely implicit solvent model returns better results with less computational overhead than trying to ensure the water is fully sampled then, within the framework of this study, the entirely implicit solvent model is better. For a system in which the solvent may not be fully sampled, the 5 Å solvent sphere is likely to be more detrimental than the traditional, entirely implicit solvent model, which is insensitive to solvent under-sampling.

Nearest Water. The second rows of Figures 2 and 3, and Supporting Information Figures S1−S3, show the electrostatic fields calculated when the water molecule closest to the nitrile Nϵ is explicitly included. In all cases, the correlation with experiment is not significantly improved with respect to the entirely implicit calculations. It was hypothesized that because the nearest water molecule in the QM/MM calculations done by Layfield et al. helped account for polarization effects by including water reorientation due to protein electrostatic fields, the same may be true for a purely classical set of calculations. This hypothesis can be tested against a second experimental measurement, the value of the Stark tuning rate, $\Delta\vec{\mu}$. Using the VSE and the slope of our best-fit line, we can back-calculate the solute dielectric, or "ideal" protein dielectric (ε'), required for the best-fit line to reproduce the known experimental value of the Stark tuning rate; these are tabulated in Table 2, along with the virtual Stark tuning rates (VSTR), correlation coefficients r, and p-values. Errors on the VSTR and ε' were obtained using eq 6 (where m is the slope, r is the correlation coefficient, and n is the number of data points in the fit) as the error of the fitted slopes.

$$\sigma_m = \frac{m}{r}\frac{\sqrt{1-r^2}}{\sqrt{n-2}} \tag{6}$$

As seen in Table 2, the "ideal" protein dielectric, which is described in detail in the Supporting Information,[32] is typically slightly larger for the nearest water calculations compared to the entirely implicit solvent calculations. Since dielectric is the macroscopic analog for the molecular property of polarizability, in a system that perfectly includes all polarizability effects, the appropriate solute dielectric is 1.0 and higher dielectric values imply incomplete modeling of polarizability effects. The strategy including waters resulted in higher values of the "ideal" protein dielectric, indicating that explicit inclusion of the nearest water molecules, in addition to neither typically nor significantly improving experimental correlation, have failed to

dx.doi.org/10.1021/jp4092656 | J. Phys. Chem. B XXXX, XXX, XXX−XXX

Table 2. Virtual Stark Tuning Rate (VSTR), "Ideal" Dielectric Constants (ε'), Correlation Coefficients (r), and p-Values for APBS Calculations of Electrostatic Fields in RalGDS Mutants in the Monomeric State and Docked to Various Rap Constructs

	implicit solvent[b]							
	numeric LPBE solutions				reaction field method			
method	VSTR[a]	ε'	r	p-value	VSTR[a]	ε'	r	p-value
monomer	1.7 ± 4.9	2.3 ± 6.7	−0.172	0.74	0.99 ± 1.47	4.0 ± 5.9	−0.319	0.53
WT	0.29 ± 0.21	13 ± 10	−0.565	0.22	0.36 ± 0.22	11 ± 7	−0.633	0.15
WT docked	0.36 ± 0.19	11 ± 6	−0.684	0.17	0.66 ± 0.72	6.0 ± 6.5	−0.417	0.46
E30D	0.46 ± 0.33	8.6 ± 6.2	−0.568	0.22	0.26 ± 0.09	15 ± 5	−0.83	0.02
E30D docked	0.60 ± 0.13	6.6 ± 1.5	−0.913	0.01	0.76 ± 0.70	5.2 ± 4.8	−0.475	0.39
K31E	1.5 ± 1.4	2.6 ± 2.5	−0.462	0.34	0.95 ± 0.40	4.2 ± 1.7	−0.768	0.05
K31E docked	0.62 ± 0.52	6.4 ± 5.3	−0.513	0.35	1.1 ± 1.5	3.5 ± 5.1	−0.336	0.56
E30D/K31E	0.54 ± 0.47	7.3 ± 6.4	−0.5	0.29	0.40 ± 0.30	9.9 ± 7.4	−0.556	0.23
E30D/K31E docked	0.34 ± 0.13	12 ± 4	−0.803	0.07	0.49 ± 0.19	8.1 ± 3.1	−0.792	0.07
	5 Å explicit solvent sphere							
	numeric LPBE solutions				reaction field method			
method	VSTR[a]	ε'	r	p-value	VSTR[a]	ε'	r	p-value
monomer	0.77 ± 0.79	5.1 ± 5.3	−0.438	0.37	0.55 ± 0.27	7.1 ± 3.5	−0.714	0.09
WT	0.80 ± 1.47	4.9 ± 9.1	−0.263	0.61	0.89 ± 1.16	4.4 ± 5.8	−0.359	0.47
WT docked	0.32 ± 0.12	12 ± 5	−0.805	0.07	0.57 ± 0.45	7.0 ± 5.5	−0.536	0.32
E30D	0.37 ± 0.21	11 ± 6	−0.656	0.13	0.23 ± 010	17 ± 7	−0.769	0.05
E30D docked	0.50 ± 0.21	8.0 ± 3.3	−0.772	0.09	0.63 ± 0.61	6.3 ± 6.1	−0.457	0.41
K31E	−2.0 ± 3.6	−2.0 ± 3.6	0.266	0.60	11 ± 40	0.37 ± 1.32	−0.135	0.79
K31E docked	0.46 ± 0.16	8.6 ± 3.1	−0.816	0.06	0.77 ± 0.55	5.2 ± 3.7	−0.571	0.28
E30D/K31E	4.7 ± 40.6	0.85 ± 7.25	−0.058	0.91	0.91 ± 1.74	4.3 ± 8.3	−0.253	0.62
E30D/K31E docked	0.30 ± 0.10	13 ± 4	−0.839	0.04	0.43 ± 0.23	9.2 ± 4.9	−0.685	0.16
	nearest water molecule							
	numeric LPBE solutions				reaction field method			
method	VSTR[a]	ε'	r	p-value	VSTR[a]	ε'	r	p-value
monomer	1.6 ± 4.5	2.5 ± 6.9	−0.176	0.73	0.92 ± 1.38	4.3 ± 6.4	−0.317	0.53
WT	0.28 ± 0.20	14 ± 10	−0.572	0.21	0.33 ± 0.18	12 ± 7	−0.676	0.12
WT docked	0.35 ± 0.18	11 ± 6	−0.688	0.16	0.63 ± 0.67	6.3 ± 6.7	−0.426	0.45
E30D	0.42 ± 0.27	9.4 ± 6.0	−0.617	0.17	0.25 ± 0.08	16 ± 4.9	−0.852	0.02
E30D docked	0.55 ± 0.13	7.2 ± 1.7	−0.905	0.01	0.69 ± 0.58	5.8 ± 4.8	−0.511	0.35
K31E	1.1 ± 0.8	3.8 ± 2.6	−0.573	0.21	0.72 ± 0.28	5.5 ± 2.1	−0.79	0.04
K31E docked	0.57 ± 0.48	6.9 ± 5.8	−0.511	0.35	1.0 ± 1.4	3.9 ± 5.5	−0.341	0.56
E30D/K31E	0.59 ± 0.65	6.7 ± 7.4	−0.412	0.40	0.41 ± 0.37	9.6 ± 8.7	−0.487	0.31
E30D/K31E docked	0.33 ± 0.11	12 ± 4	−0.824	0.05	0.48 ± 0.19	8.2 ± 3.2	−0.789	0.08
	hydrogen-bonding water molecule							
	numeric LPBE solutions				reaction field method			
method	VSTR[a]	ε'	r	p-value	VSTR[a]	ε'	r	p-value
monomer	1.7 ± 4.9	2.3 ± 6.7	−0.171	0.74	0.97 ± 1.46	4.1 ± 6.2	−0.315	0.53
WT	0.29 ± 0.21	14 ± 10	−0.57	0.21	0.35 ± 0.20	11 ± 7	−0.652	0.14
WT docked	0.36 ± 0.19	11 ± 5.8	−0.689	0.16	0.65 ± 0.70	6.1 ± 6.5	−0.423	0.46
E30D	0.46 ± 0.33	8.6 ± 6.3	−0.567	0.22	0.26 ± 0.09	15 ± 5	−0.836	0.02
E30D docked	0.59 ± 0.13	6.7 ± 1.5	−0.912	0.01	0.74 ± 0.66	5.3 ± 4.8	−0.489	0.38
K31E	1.4 ± 1.3	2.8 ± 2.6	−0.481	0.31	0.90 ± 0.37	4.4 ± 1.8	−0.772	0.05
K31E docked	0.61 ± 0.52	6.5 ± 5.5	−0.508	0.35	1.1 ± 1.6	3.6 ± 5.1	−0.334	0.57
E30D/K31E	0.51 ± 0.43	7.7 ± 6.5	−0.513	0.28	0.38 ± 0.28	10 ± 8	−0.565	0.22
E30D/K31E docked	0.33 ± 0.12	12 ± 5	−0.801	0.07	0.47 ± 0.18	8.3 ± 3.2	−0.797	0.07

[a]Virtual Stark tuning rate, in units of $cm^{-1}/(k_bT/eÅ)$. [b]Previously reported results

capture previously excluded polarizability effects in the continuum calculation.

Hydrogen-Bonding Water. The third rows of Figures 2 and 3 and Supporting Information Figures S1−S3, show the electrostatic fields calculated when the water molecule hydrogen-bonding to the nitrile Nε (N···H distance ≤2.25 Å, N−H−O smallest bond angle ≥138°) is explicitly included. In all cases, the correlation with experiment is not significantly different from the entirely implicit calculations. This is due to the relatively few number of frames in which hydrogen bonding is actually observed. The RalGDS monomers had the highest occurrence, with 10.69% of all frames having a hydrogen-bonding water. The docked complexes showed fewer frames with hydrogen bonding atoms; WT Rap, Rap E30D/K31E, Rap

dx.doi.org/10.1021/jp4092656 | J. Phys. Chem. B XXXX, XXX, XXX−XXX

K31E, and Rap E30D each had 9.92, 9.39, 9.36, and 8.63%, respectively, of frames with a hydrogen-bonded water molecule. The frequency of frames containing hydrogen-bonding water for each system/probe combination is shown in Supporting Information Table S1. Because such a small number of frames even have a hydrogen-bonding water, the field calculations are dominated by frames with zero explicit water molecules, identical to those in the original calculations, and therefore, the Boltzmann-weighted average is nearly identical to the original calculations. There are not enough frames containing a water molecule to significantly shift the electrostatic field experienced by the nitrile probe.

In summary, although the 5 Å water sphere calculation significantly altered the calculated electrostatic field, a targeted, enhanced molecular dynamics strategy which may leave solvent under-sampled is detrimental to the overall quality of the calculations in a way not observed when using an entirely implicit solvent model. Additionally, including only the nearest water molecules or water molecules hydrogen-bonding to the nitrile Nε also does not appear to significantly improve experimental correlation, and for absolute field calculations using a LPBE model, no consideration for interfacial or near-site-of-interest water is necessary.

B. Calculations of Field Differences. Figure 6 and Supporting Information Figures S9−S11, compare the calculated relative electrostatic fields due to docking at the nitrile bond midpoint projected along the nitrile bond vector using the various explicit solvent methods (blue) to the experimentally observed nitrile vibrational absorption frequencies for RalGDS docked to WT Rap, and RalGDS docked to E30D, K31E, and E30D/K31E, respectively. As in the absolute calculations, error bars have been omitted for clarity and are approximately ±1 cm^{-1} in the *x*-axis and ±6.5 k_bT/eÅ in the *y*-axis. Previously published results using entirely implicit solvent are also shown in red for comparison. Results using both the numeric LBPE solutions (left column) as well as the reaction field method (right column) are presented. Consistent with our previous study, the numeric method yields higher correlation to experiment than the reaction field method for the relative calculations, and therefore, further discussion of the relative field calculations is limited to those obtained by the numeric method.

5 Å Sphere. The top rows of Figure 6 and Supporting Information Figures S9−S11, show the relative electrostatic fields due to RalGDS docking to the WT Rap, Rap E30D, Rap K31E, and Rap E30D/K31E, respectively, calculated when all water molecules within 5 Å of the nitrile Nε atom are explicitly included. Although the explicit solvent sphere was largely a failure for the absolute field calculations, the relative field calculations show the same recovery of correlation we previously reported.[32] The numeric relative fields were significantly more correlated to the experimental vibrational energies of the nitrile probe than the reaction field method absolute fields for the WT Rap, Rap K31E, and Rap E30D/K31E. The numeric relative field for RalGDS docked to Rap E30D was approximately the same as the reaction field correlation. The increased correlations are unlikely to be purely an artifact of the better-correlated RalGDS monomer calculation because of the poor correlation of the absolute field calculations for all of the docked complexes. As before, when taking the *difference* in electrostatic fields obtained from the LPBE, cancellation of errors in the continuum calculations was observed. These observations further support the conclusion of

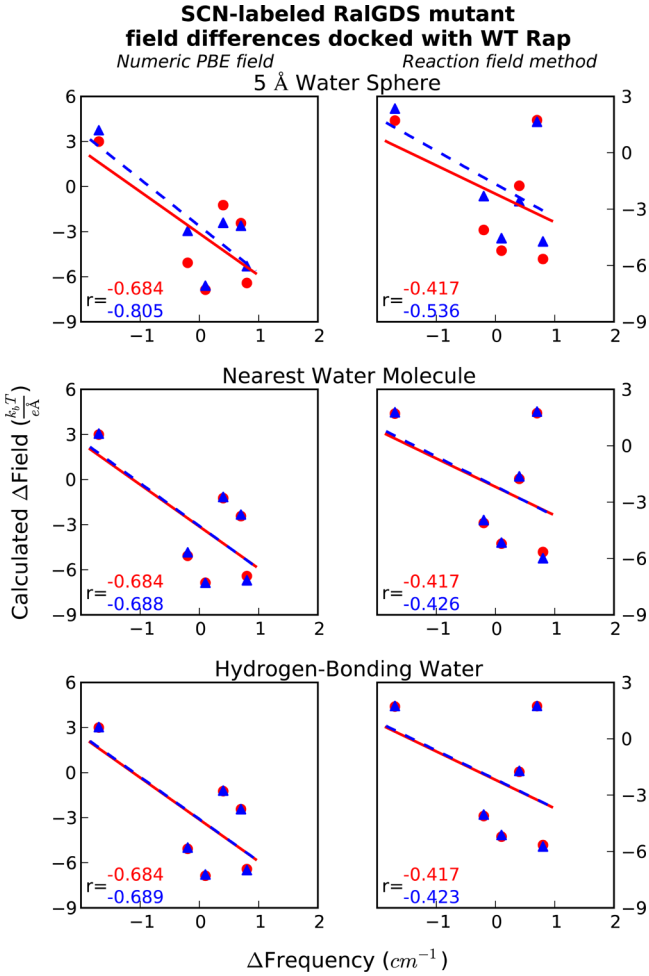

Figure 6. Relative field calculations using the numeric LPBE solutions (left column) and from the numeric reaction field method (right column) compared to the experimental changes in frequencies for various nitrile probe locations on RalGDS upon docking to WT Rap: red, originally reported, entirely implicit solvent fields; blue, fields using the solvent selection model described by the row subheading. Correlation coefficients are listed in the bottom left corner in the corresponding color. Standard deviations are approximately ±1 cm^{-1} and ±6.5 k_bT/eÅ.

our previous investigation; some nonphysical characteristic or important, excluded physical characteristics not adequately addressed in the absolute calculations can be canceled out by the subtraction of fields in a comparison of two similar but slightly different states. Additionally, we see slightly greater experimental correlation using the explicit solvent sphere for the relative field calculations than when using the entirely implicit model. However, if trying to efficiently maximizing both absolute and relative field correlations, the additional computational cost of performing both entirely implicit calculations and the 5 Å sphere calculations favors the use of entirely implicit solvent.

Nearest Water and Hydrogen-Bonding Water. The second rows of Figure 6 and Supporting Information Figures S9−S11, show the relative electrostatic fields due to RalGDS docking to the WT Rap, Rap E30D, Rap K31E, and Rap E30D/K31E, respectively, calculated with the water molecule nearest the nitrile Nε atom explicitly included, while the third rows show the relative fields calculated explicitly including only hydrogen-bonding waters. In both methods, the relative fields and the

dx.doi.org/10.1021/jp4092656 | J. Phys. Chem. B XXXX, XXX, XXX−XXX

"ideal" dielectric constants estimated from the calculation are nearly identical to the original calculations with no explicit water molecules included. Although the nearest water method is guaranteed to have an additional source of charge close to the nitrile, the values for the relative fields were approximately the same as in the implicit model. This suggests that any effect that the nearest water molecule may have on the electrostatic environment of the nitrile probe is just as well modeled explicitly as implicit bulk water. This in turn implies that treating bulk water explicitly as part of the solute dielectric does not detract from the overall quality of the calculation and there is some leeway in assigning bulk versus hydration water. For relative field calculations, no consideration for nearest or hydrogen-bonding water is necessary.

For quantifying *changes* in electrostatic fields with *changes* in vibrational absorption frequency due to docking to another protein, explicitly including a 5 Å solvent sphere near the location-of-interest was beneficial to the overall correlation, but because of the poor absolute correlation, comes at an additional cost that may not justify the small increase in correlation over using entirely implicit solvent.

CONCLUSION

When calculating the absolute electrostatic environment of a nitrile covalently bound to the surface of a protein using the LPBE, unlike the results reported for QM/MM vibrational spectra calculations,[19] explicit solvent near the vibrational chromophore should not be included in lieu of an implicit model when solvent sampling may be an issue. We do not see any consistent, significant increase in correlation by explicitly including all water near the nitrile probe, the closest water molecule to the nitrile probe, or water hydrogen bonding to the probe. However, for comparing vibrational absorption energy shifts due to docking, the inclusion of explicit solvent yielded slightly improved results for the 5 Å solvent spheres and nearly identical results for the nearest water and hydrogen-bonding waters compared to the wholly implicit solvent calculation. In computing changes in protein electrostatics due to some perturbation using the LPBE model, there appears to be neither significant, consistent advantage nor disadvantage to explicitly modeling the hydration water when there is little to no persistent hydrogen bonding and the desired information is the difference between two calculations, not an absolute value of the electrostatic field. However, explicitly including water requires an additional preparation step, selecting the waters and, thus, is slightly more computationally expensive for very little additional information and significantly more expensive if the absolute fields are also important. We find that, although QM/MM calculations of the nitrile absorption frequency are largely benefitted by the inclusion of water near the nitrile probe,[19] explicit definition of water molecules near the vibrational Stark probe typically yields neither significant improvement nor deterioration of the predictive capability of vibrational Stark shifts using the LPBE electric field difference calculations and is likely not necessary for future, similar calculations. Additionally, because the use of explicit water does not address the lack of atomic polarizability and the choice of the protein dielectric is arbitrary, additional studies will be aimed at investigating the use of the polarizable model AMOEBA.[65−67] To address the possibly poor solvent sampling, our laboratory is currently investigating the use of other enhanced sampling techniques, such as replica exchange molecular dynamics (REMD).[68,69]

ASSOCIATED CONTENT

Supporting Information

Additional figures containing calculated electrostatic fields for labeled RalGDS mutants docked to Rap E30D, Rap K31E, and Rap E30D/K31E. This material is available free of charge via the Internet at http://pubs.acs.org.

AUTHOR INFORMATION

Corresponding Author

*E-mail: lwebb@cm.utexas.edu.

Notes

The authors declare no competing financial interest.

ACKNOWLEDGMENTS

This work was supported by the Burroughs Wellcome Fund (1007207.01), The Welch Foundation (F-1722), and OpenEye Scientific Software. L.J.W. holds a Career Award at the Scientific Interface from the Burroughs Wellcome Fund and is an Alfred P. Sloan Research Fellow. The authors acknowledge the Texas Advanced Computing Center (TACC) at The University of Texas at Austin for providing high-performance computing resources that have contributed to the results reported within this paper.

REFERENCES

(1) Ensign, D. L.; Webb, L. J. Factors Determining Electrostatic Fields at the Ras/Effector Interface. *Proteins* **2011**, *79*, 3511−3524.

(2) Pearson, J. G.; Oldfield, E.; Lee, F. S.; Warshel, A. Chemical-Shifts in Proteins: A Shielding Trajectory Analysis of the Fluorine Nuclear-Magnetic-Resonance Spectrum of the *Escherichia coli* Galactose Binding-Protein Using a Multipole Shielding Polarizability Local Reaction Field Molecular-Dynamics Approach. *J. Am. Chem. Soc.* **1993**, *115* (15), 6851−6862.

(3) Mobley, D. L.; Graves, A. P.; Chodera, J. D.; McReynolds, A. C.; Shoichet, B. K.; Dill, K. A. Predicting Absolute Ligand Binding Free Energies to a Simple Model Site. *J. Mol. Biol.* **2007**, *371* (4), 1118−1134.

(4) Danielson, M. A.; Falke, J. J. Use of ^{19}F NMR To Probe Protein Structure and Conformational Changes. *Annu. Rev. Biophys. Biomol. Struct.* **1996**, *25*, 163−195.

(5) Schutz, C. N.; Warshel, A. What are Dielectric "Constants" of Proteins and How to Validate Electrostatic Models? *Proteins* **2001**, *44*, 400−417.

(6) Forsyth, W. R.; Antosiewicz, J. M.; Robertson, A. D. Empirical Relationships between Protein Structure and Carboxyl pK_a Values in Proteins. *Proteins: Struct., Funct., Bioinf.* **2002**, *48* (2), 388−403.

(7) Matousek, W. M.; Ciani, B.; Fitch, C. A.; Garcia-Moreno, B.; Kammerer, R. A.; Alexandrescu, A. T. Electrostatic Contributions to the Stability of the GCN4 Leucine Zipper Structure. *J. Mol. Biol.* **2007**, *374* (1), 206−219.

(8) Baran, K. L.; Chimenti, M. S.; Schlessman, J. L.; Fitch, C. A.; Herbst, K. J.; Garcia-Moreno, B. E. Electrostatic Effects in a Network of Polar and Ionizable Groups in Staphylococcal Nuclease. *J. Mol. Biol.* **2008**, *379* (5), 1045−1062.

(9) Castaneda, C. A.; Fitch, C. A.; Majumdar, A.; Khangulov, V.; Schlessman, J. L.; Garcia-Moreno, B. E. Molecular Determinants of the pK_a Values of Asp and Glu Residues in Staphylococcal Nuclease. *Proteins: Struct., Funct., Bioinf.* **2009**, *77* (3), 570−588.

(10) Harms, M. J.; Castaneda, C. A.; Schlessman, J. L.; Sue, G. R.; Isom, D. G.; Cannon, B. R.; Garcia-Moreno, B. The pK_a Values of Acidic and Basic Residues Buried at the Same Internal Location in a Protein are Governed by Different Factors. *J. Mol. Biol.* **2009**, *389* (1), 34−47.

(11) Gunner, M. R.; Nicholls, A.; Honig, B. Electrostatic Potentials in *Rhodopseudomonas viridis* Reaction Centers: Implications for the

Driving Force and Directionality of Electron Transfer. *J. Phys. Chem.* **1996**, *100*, 4277−4291.
(12) Nielsen, J. E.; Andersen, K. V.; Honig, B.; Hooft, R. W. W.; Klebe, G.; Vriend, G.; Wade, R. C. Improving Macromolecular Electrostatics Calculations. *Protein Eng.* **1999**, *12*, 657−662.
(13) Nielsen, J. E.; Gunner, M. R.; Garcia-Moreno, E. B. The pK_a Cooperative: A Collaborative Effort to Advance Structure-Based Calculations of pK_a Values and Electrostatic Effects in Proteins. *Proteins: Struct., Funct., Bioinf.* **2011**, *79* (12), 3249−3259.
(14) Nielsen, J. P.; Petersen, H. H. Objective Measurement of Health Pigs: Application of Acute Phase Proteins. *Acta Vet. Scand.* **2003**, 125−125.
(15) Alexov, E.; Mehler, E. L.; Baker, N.; Baptista, A. M.; Huang, Y.; Milletti, F.; Nielsen, J. E.; Farrell, D.; Carstensen, T.; Olsson, M. H. M.; et al. Progress in the Prediction of pK_a Values in Proteins. *Proteins: Struct., Funct., Bioinf.* **2011**, *79* (12), 3260−3275.
(16) Jiao, D.; Golubkov, P. A.; Darden, T. A.; Ren, P. Calculation of Protein-Ligand Binding Free Energy by Using a Polarizable Potential. *Proc. Natl. Acad. Sci. U.S.A.* **2008**, *105*, 6290−6295.
(17) Jiao, D.; Zhang, J. J.; Duke, R. E.; Li, G. H.; Schnieders, M. J.; Ren, P. Y. Trypsin-Ligand Binding Free Energies from Explicit and Implicit Solvent Simulations with Polarizable Potential. *J. Comput. Chem.* **2009**, *30* (11), 1701−1711.
(18) Baker, N. A. Poisson-Boltzmann Methods for Biomolecular Electrostatics. *Method Enzymol.* **2004**, *383*, 94−+.
(19) Layfield, J. P.; Hammes-Schiffer, S. Calculation of Vibrational Shifts of Nitrile Probes in the Active Site of Ketosteroid Isomerase upon Ligand Binding. *J. Am. Chem. Soc.* **2013**, *135* (2), 717−725.
(20) Lindquist, B. A.; Corcelli, S. A. Nitrile Groups as Vibrational Probes: Calculations of the CN Infrared Absorption Line Shape of Acetonitrile in Water and Tetrahydrofuran. *J. Phys. Chem. B* **2008**, *112*, 6301−6303.
(21) Lindquist, B. A.; Furse, K. E.; Corcelli, S. A. Nitrile Groups as Vibrational Probes of Biomolecular Structure and Dynamics: An Overview. *Phys. Chem. Chem. Phys.* **2009**, *11*, 8119−8132.
(22) Lindquist, B. A.; Haws, R. T.; Corcelli, S. A. Optimized Quantum Mechanics/Molecular Mechanics Strategies for Nitrile Vibrational Probes: Acetronitrile and *para*-Tolunitrile in Water and Tetrahydrofuran. *J. Phys. Chem. B* **2008**, *112*, 13991−14001.
(23) Teixeira, V. H.; Cunha, C. A.; Machuqueiro, M.; Oliveira, A. S. F.; Victor, B. L.; Soares, C. M.; Baptista, A. M. On the Use of Different Dielectric Constants for Computing Individual and Pairwise Terms in Poisson-Boltzmann Studies of Protein Ionization Equilibrium. *J. Phys. Chem. B* **2005**, *109* (30), 14691−14706.
(24) Warshel, A.; Levitt, M. Theoretical Studies of Enzymic Reactions: Dielectric, Electrostatic and Steric Stabilization of the Carbonium Ion in the Reaction of Lysozyme. *J. Mol. Biol.* **1976**, *103*, 227−249.
(25) Warshel, A.; Papazyan, A. Electrostatic Effects in Macromolecules: Fundamental Concepts and Practical Modeling. *Curr. Opin. Struct. Biol.* **1998**, *8*, 211−217.
(26) Warshel, A.; Sharma, P. K.; Kato, M.; Parson, W. W. Modeling Electrostatic Effects in Proteins. *Biochim. Biophys. Acta* **2006**, *1764*, 1647−1676.
(27) Choi, J. H.; Oh, K. I.; Lee, H.; Lee, C.; Cho, M. Nitrile and Thiocyanate IR Probes: Quantum Chemistry Calculation Studies and Multivariate Least-Square Fitting Analysis. *J. Chem. Phys.* **2008**, *128*, 134506.
(28) Urbanek, D. C.; Vorobyev, D. Y.; Serrano, A. L.; Gai, F. The Two-Dimensional Virbational Echo of a Nitrile Probe of the Villin HP35 Protein. *J. Phys. Chem. Lett.* **2010**, *1*, 3311−3315.
(29) Waegele, M. M.; Gai, F. Computational Modeling of the Nitrile Stretching Vibration of 5-Cyanoindole in Water. *J. Phys. Chem. Lett.* **2010**, *1*, 781−786.
(30) Waegele, M. M.; Gai, F.; Culik, R. M. Site-Specific Spectroscopic Reporters of the Local Electric Field, Hydration, Structure, and Dynamics of Biomolecules. *J. Phys. Chem. Lett.* **2011**, *2*, 2598−2609.
(31) Waegele, M. M.; Tucker, M. J.; Gai, F. 5-Cyanotryptophan as an Infrared Probe of Local Hydration Status of Proteins. *Chem. Phys. Lett.* **2009**, *478*, 249−253.
(32) Ritchie, A. W.; Webb, L. J. Optimizing Electrostatic Field Calculations with the Adaptive Poisson-Boltzmann Solver to Predict Electric Fields at Protein−Protein Interfaces I: Sampling and Focusing. *J. Phys. Chem. B* **2013**, *117*, 11473−11489.
(33) Honig, B.; Nicholls, A. Classical Electrostatics in Biology and Chemistry. *Science* **1995**, *268* (5214), 1144−1149.
(34) Baker, N. A.; Sept, D.; Joseph, S.; Holst, M. J.; McCammon, J. A. Electrostatics of Nanosystems: Application to Microtubles and the Ribosome. *Proc. Natl. Acad. Sci. U.S.A.* **2001**, *98*, 10037−10041.
(35) Holst, M.; Saied, F. Multigrid Solution of the Poisson-Boltzmann Equation. *J. Comput. Chem.* **1993**, *14* (1), 105−113.
(36) Holst, M. J.; Saied, F. Numerical-Solution of the Nonlinear Poisson-Boltzmann Equation: Developing More Robust and Efficient Methods. *J. Comput. Chem.* **1995**, *16* (3), 337−364.
(37) Cerutti, D. S.; Baker, N. A.; McCammon, J. A. Solvent Reaction Field Potential inside an Uncharged Globular Protein: A Bridge between Implicit and Explicit Solvent Models. *J. Chem. Phys.* **2007**, *127*, 1−28, DOI: 10.1063/1.2771171.
(38) Andrews, S. S.; Boxer, S. G. Vibrational Stark Effects of Nitriles I. Methods and Experimental Results. *J. Phys. Chem. A* **2000**, *104*, 11853−11863.
(39) Andrews, S. S.; Boxer, S. G. Vibrational Stark Effects of Nitriles II. Physical Origins of Stark Effects from Experiment and Perturbation Models. *J. Phys. Chem. A* **2002**, *106*, 469−477.
(40) Park, E. S.; Andrews, S. S.; Hu, R. B.; Boxer, S. G. Vibrational Stark Spectroscopy in Proteins: A Probe and Calibration for Electrostatic Fields. *J. Phys. Chem. B* **1999**, *103*, 9813−9817.
(41) Ragain, C. M.; Newberry, R. W.; Ritchie, A. W.; Webb, L. J. Role of Electrostatics in Differential Binding of RaIGDS to Rap Mutations E30D and K31E Investigated by Vibrational Spectroscopy of Thiocyanate Probes. *J. Phys. Chem. B* **2012**, *116* (31), 9326−9336.
(42) Stafford, A. J.; Ensign, D. L.; Webb, L. J. Vibrational Stark Effect Spectroscopy at the Interface of Ras and Rap1A Bound to the Ras Binding Domain of RalGDS Reveals an Electrostatic Mechanism for Protein−Protein Interaction. *J. Phys. Chem. B* **2010**, *114*, 15331−15344.
(43) Suydam, I. T.; Boxer, S. G. Vibrational Stark Effects Calibrate the Sensitivity of Vibrational Probes for Electric Fields in Proteins. *Biochemistry* **2003**, *42*, 12050−12055.
(44) Webb, L. J.; Boxer, S. G. Electrostatic Fields Near the Active Site of Human Aldose Reductase: 1. New Inhibitors and Vibrational Stark Effect Measurements. *Biochemistry* **2008**, *47*, 1588−1598.
(45) Neves-Petersen, M. T.; Petersen, S. B. Protein Electrostatics: A review of the equations and methods used to model electrostatic equations in biomolecules. *Applications in Biotechnology. Biotechnology Annual Review*; Elsevier: New York, 2003; Vol. *9*, pp 315−395.
(46) Chen, X. F.; Weber, I.; Harrison, R. W. Hydration Water and Bulk Water in Proteins Have Distinct Properties in Radial Distributions Calculated from 105 Atomic Resolution Crystal Structures. *J. Phys. Chem. B* **2008**, *112* (38), 12073−12080.
(47) Higo, J.; Nakasako, M. Hydration Structure of Human Lysozyme Investigated by Molecular Dynamics Simulation and Cryogenic X-ray Crystal Structure Analyses: On the Correlation between Crystal Water Sites, Solvent Density, And Solvent Dipole. *J. Comput. Chem.* **2002**, *23* (14), 1323−1336.
(48) Nakasako, M. Large-Scale Networks of Hydration Water Molecules around Bovine β-Trypsin Revealed by Cryogenic X-ray Crystal Structure Analysis. *J. Mol. Biol.* **1999**, *289* (3), 547−564.
(49) Yokomizo, T.; Higo, J.; Nakasako, M. Patterns and Networks of Hydrogen-Bonds in the Hydration Structure of Human Lysozyme. *Chem. Phys. Lett.* **2005**, *410* (1−3), 31−35.
(50) Sheu, S. Y.; Yang, D. Y. Determination of Protein Surface Hydration Shell Free Energy of Water Motion: Theoretical Study and Molecular Dynamics Simulation. *J. Phys. Chem. B* **2010**, *114* (49), 16558−16566.

(51) Chung, E.; Henriques, D.; Renzoni, D.; Zvelebil, M.; Bradshaw, J. M.; Waksman, G.; Robinson, C. V.; Ladbury, J. E. Mass Spectrometric and Thermodynamic Studies Reveal the Role of Water Molecules in Complexes Formed between SH_2 Domains and Tyrosyl Phosphopeptides. *Struct. Fold. Des.* **1998**, *6* (9), 1141−1151.
(52) Funahashi, J.; Takano, K.; Yamagata, Y.; Yutani, K. Positive Contribution of Hydration Structure on the Surface of Human Lysozyme to the Conformational Stability. *J. Biol. Chem.* **2002**, *277* (24), 21792−21800.
(53) Fennell, C. J.; Kehoe, C. W.; Dill, K. A. Modeling Aqueous Solvation with Semi-Explicit Assembly. *Proc. Natl. Acad. Sci. U.S.A.* **2011**, *108* (8), 3234−3239.
(54) Duan, Y.; Wu, C.; Chowdhury, S.; Lee, M. C.; Xiong, G.; Zhang, W.; Yang, R.; Cieplak, P.; Luo, R.; Lee, T.; et al. A Point-Charge Force Field for Molecular Mechanics Simulations of Proteins Based on Condensed-Phase Quantum Mechanical Calculations. *J. Comput. Chem.* **2003**, *24*, 1999−2012.
(55) van der Spoel, D.; Lindahl, E.; Hess, B.; Groenhof, G.; Mark, A. E.; Berendsen, H. J. C. GROMACS: Fast, Flexible, and Free. *J. Comput. Chem.* **2005**, *26*, 1701−1718.
(56) Berendsen, H. J. C.; Spoel, D. v. d.; Drunen, R. v. GROMACS: A Message-Passing Parallel Molecular Dynamics Implementation. *Comput. Phys. Commun.* **1995**, *91*, 43−56.
(57) Hess, B.; Kutzner, C.; Spoel, D. v. d.; Lindahl, E. GROMACS 4: Algorithms for Highly Efficient, Load-Balanced, And Scalable Molecular Simulation. *J. Chem. Theory Comput.* **2008**, *4*, 435−447.
(58) Lindahl, E.; Hess, B.; Spoel, D. v. d. GROMACS 3.0: A Package for Molecular Simulation and Trajectory Analysis. *J. Mol. Model.* **2001**, *7*, 306−317.
(59) Roux, B. The Calculation of the Potential of Mean Force Using Computer Simulations. *Comput. Phys. Commun.* **1995**, *91*, 275−282.
(60) Gallicchio, E.; Andrec, M.; Felts, A. K.; Levy, R. M. Temperature Weighted Histogram Analysis Method, Replica Exchange, and Transition Paths. *J. Phys. Chem. B* **2005**, *109*, 6722−6731.
(61) Dolinsky, T. J.; Czodrowski, P.; Li, H.; Nielsen, J. E.; Jensen, J. H.; Klebe, G.; Baker, N. A. PDB2PQR: Expanding and Upgrading Automated Preparation of Biomolecular Structures for Molecular Simulations. *Nucleic Acids Res.* **2007**, *35*, W522−W525.
(62) Dolinsky, T. J.; Nielsen, J. E.; McCammon, J. A.; Baker, N. A. PDB2PQR: An Automated Pipeline for the Setup of Poisson-Boltzmann Electrostatics Calculations. *Nucleic Acids Res.* **2004**, *32*, W665−W667.
(63) Le Questel, J. Y.; Berthelot, M.; Laurence, C. Hydrogen-Bond Acceptor Properties of Nitriles: A Combined Crystallographic and Ab Initio Theoretical Investigation. *J. Phys. Org. Chem.* **2000**, *13* (6), 347−358.
(64) Fried, S. D.; Bagchi, S.; Boxer, S. G. Measuring Electrostatic Fields in Both Hydrogen-Bonding and Non-Hydrogen-Bonding Environments Using Carbonyl Vibrational Probes. *J. Am. Chem. Soc.* **2013**, *135* (30), 11181−11192.
(65) Ponder, J. W.; Wu, C.; Ren, P.; Pande, V. S.; Chodera, J. D.; Schnieders, M. J.; Haque, I.; Mobley, D. L.; Lambrecht, D. S.; DiStasio, R. A.; et al. Current Status of the AMOEBA Polarizable Force Field. *J. Phys. Chem. B* **2010**, *114*, 2549−2564.
(66) Ren, P. Y.; Ponder, J. W. Polarizable atomic multipole water model for molecular mechanics simulation. *J. Phys. Chem. B* **2003**, *107* (24), 5933−5947.
(67) Schnieders, M. J.; Baker, N. A.; Ren, P.; Ponder, J. W. Polarizable Atomic Multipole Solutes in a Poisson-Boltzmann Continuum. *J. Chem. Phys.* **2007**, *126*, 124114−1−47.
(68) Hukushima, K.; Nemoto, K. Exchange Monte Carlo Method and Application to Spin Glass Simulations. *J. Phys. Soc. Jpn.* **1996**, *65*, 1604−1608.
(69) Sugita, Y.; Okamoto, Y. Replica-Exchange Molecular Dynamics Method for Protein Folding. *Chem. Phys. Lett.* **1999**, *314*, 141−151.